Biomedical Optics EXPRESS

Time-resolved singlet-oxygen luminescence detection with an efficient and practical semiconductor single-photon detector

Gianluca Boso,[1,*] Damei Ke,[2] Boris Korzh,[1] Jordan Bouilloux,[2] Norbert Lange,[2] and Hugo Zbinden[1]

[1]*Group of Applied Physics, University of Geneva, Chemin de Pinchat 22, Genève 4, CH-1211, Switzerland*
[2]*School of Pharmaceutical Sciences, University of Geneva, University of Lausanne, Quai Ernest Ansermet 30, Genève 4, CH-1211, Switzerland*
[*]*gianluca.boso@unige.ch*

Abstract: In clinical applications, such as PhotoDynamic Therapy, direct singlet-oxygen detection through its luminescence in the near-infrared range (1270 nm) has been a challenging task due to its low emission probability and the lack of suitable single-photon detectors. Here, we propose a practical setup based on a negative-feedback avalanche diode detector that is a viable alternative to the current state-of-the art for different clinical scenarios, especially where geometric collection efficiency is limited (e.g. fiber-based systems, confocal microscopy, scanning systems etc.). The proposed setup is characterized with Rose Bengal as a standard photosensitizer and it is used to measure the singlet-oxygen quantum yield of a new set of photosensitizers for site-selective photodynamic therapy.

OCIS codes: (230.5160) Photodetectors; (270.5570) Quantum detectors; (030.5260) Photon counting; (170.3880) Medical and biological imaging; (170.6920) Time-resolved imaging; (170.6280) Spectroscopy, fluorescence and luminescence; (250.5230) Photoluminescence; (350.5130) Photochemistry; (170.5180) Photodynamic therapy.

References and links

1. M. B. Ericson, A. M. Wennberg, and O. Larkö, "Review of photodynamic therapy in actinic keratosis and basal cell carcinoma," Ther. Clin. Risk Manag. **4**(1), 1–9 (2008).
2. M. F. Zuluaga, D. Gabriel, and N. Lange, "Enhanced prostate cancer targeting by modified protease sensitive photosensitizer prodrugs," Mol. Pharm. **9**(6), 1570–1579 (2012).
3. D. E. J. G. J. Dolmans, D. Fukumura, and R. K. Jain, "Photodynamic therapy for cancer," Nat. Rev. Cancer **3**(5), 380–387 (2003).
4. S. B. Brown, E. A. Brown, and I. Walker, "The present and future role of photodynamic therapy in cancer treatment," Lancet Oncol. **5**(8), 497–508 (2004).
5. U. Schmidt-Erfurth and T. Hasan, "Mechanisms of action of photodynamic therapy with verteporfin for the treatment of age-related macular degeneration," Surv. Ophthalmol. **45**(3), 195–214 (2000).
6. C. Schweitzer and R. Schmidt, "Physical mechanisms of generation and deactivation of singlet oxygen," Chem. Rev. **103**(5), 1685–1758 (2003).
7. P. R. Ogilby, "Singlet oxygen: there is indeed something new under the sun," Chem. Soc. Rev. **39**(8), 3181–3209 (2010).
8. M. T. Jarvi, M. J. Niedre, M. S. Patterson, and B. C. Wilson, "Singlet oxygen luminescence dosimetry (SOLD) for photodynamic therapy: current status, challenges and future prospects," Photochem. Photobiol. **82**(5), 1198–1210 (2006).
9. I. Coto Hernández, M. Buttafava, G. Boso, A. Diaspro, A. Tosi, and G. Vicidomini, "Gated STED microscopy with time-gated single-photon avalanche diode," Biomed. Opt. Express **6**(6), 2258–2267 (2015).
10. M. Mazurenka, L. Di Sieno, G. Boso, D. Contini, A. Pifferi, A. D. Mora, A. Tosi, H. Wabnitz, and R. Macdonald, "Non-contact in vivo diffuse optical imaging using a time-gated scanning system," Biomed. Opt. Express **4**(10), 2257–2268 (2013).
11. E. Alerstam, T. Svensson, S. Andersson-Engels, L. Spinelli, D. Contini, A. Dalla Mora, A. Tosi, F. Zappa, and A. Pifferi, "Single-fiber diffuse optical time-of-flight spectroscopy," Opt. Lett. **37**(14), 2877–2879 (2012).
12. M. Itzler, X. Jiang, M. Entwistle, K. Slomkowski, A. Tosi, F. Acerbi, F. Zappa, and S. Cova, "Advances in InGaAsP-based avalanche diode single photon detectors," J. Mod. Opt. **58**(3–4), 174–200 (2011).
13. I. Bargigia, A. Tosi, A. Bahgat Shehata, A. Della Frera, A. Farina, A. Bassi, P. Taroni, A. Dalla Mora, F. Zappa, R. Cubeddu, and A. Pifferi, "Time-resolved diffuse optical spectroscopy up to 1700 nm by means of a time-gated InGaAs/InP single-photon avalanche diode," Appl. Spectrosc. **66**(8), 944–950 (2012).

#251795 Received 14 Oct 2015; revised 17 Dec 2015; accepted 17 Dec 2015; published 23 Dec 2015

14. N. R. Gemmell, A. McCarthy, B. Liu, M. G. Tanner, S. D. Dorenbos, V. Zwiller, M. S. Patterson, G. S. Buller, B. C. Wilson, and R. H. Hadfield, "Singlet oxygen luminescence detection with a fiber-coupled superconducting nanowire single-photon detector," Opt. Express **21**(4), 5005–5013 (2013).
15. T. Lunghi, C. Barreiro, O. Guinnard, R. Houlmann, X. Jiang, M. A. Itzler, and H. Zbinden, "Free-running single-photon detection based on a negative feedback InGaAs APD," J. Mod. Opt. **59**(17), 1481–1488 (2012).
16. B. Korzh, N. Walenta, T. Lunghi, N. Gisin, and H. Zbinden, "Free-running InGaAs single photon detector with 1 dark count per second at 10% efficiency," Appl. Phys. Lett. **104**(8), 081108 (2014).
17. R. W. Redmond and J. N. Gamlin, "A compilation of singlet oxygen yields from biologically relevant molecules," Photochem. Photobiol. **70**(4), 391–475 (1999).
18. F. Wilkinson, W. P. Helman, and A. B. Ross, "Quantum yield for the photosensitized formation of the lowest electronically excited singlet state of molecular oxygen in solution," J. Phys. Chem. Ref. Data **22**(1), 113–262 (1993).
19. Y. Urano, "Novel live imaging techniques of cellular functions and in vivo tumors based on precise design of small molecule-based 'activatable' fluorescence probes," Curr. Opin. Chem. Biol. **16**(5-6), 602–608 (2012).
20. T. Ooi, T. Shibata, R. Sato, H. Ohno, S. Kinoshita, T. L. Thuoc, and S. Taguchi, "An azoreductase, aerobic NADH-dependent flavoprotein discovered from Bacillus sp.: functional expression and enzymatic characterization," Appl. Microbiol. Biotechnol. **75**(2), 377–386 (2007).
21. A. Ryan, E. Kaplan, J. C. Nebel, E. Polycarpou, V. Crescente, E. Lowe, G. M. Preston, and E. Sim, "Identification of NAD(P)H quinone oxidoreductase activity in azoreductases from P. aeruginosa: azoreductases and NAD(P)H quinone oxidoreductases belong to the same FMN-dependent superfamily of enzymes," PLoS One **9**(6), e98551 (2014).
22. M. A. Itzler, X. Jiang, B. Nyman, and K. Slomkowski, "InP-based negative feedback avalanche diodes," Proc. SPIE **7222**, 72221K (2009).
23. B. Korzh, T. Lunghi, K. Kuzmenko, G. Boso, and H. Zbinden, "Afterpulsing studies of low-noise InGaAs/InP single-photon negative-feedback avalanche diodes," J. Mod. Opt. **62**(14), 1151–1157 (2015).
24. W. Becker, *Advanced Time-Correlated Single Photon Counting Techniques* (Springer, 2005).
25. M. Niedre, M. S. Patterson, and B. C. Wilson, "Direct near-infrared luminescence detection of singlet oxygen generated by photodynamic therapy in cells in vitro and tissues in vivo," Photochem. Photobiol. **75**(4), 382–391 (2002).
26. Laser Institute of America, *American National Standard for Safe Use of Lasers in ANSI Z136.1–2000* (Laser Institute of America, 2000).
27. G. Wagnières, S. Cheng, M. Zellweger, N. Utke, D. Braichotte, J. P. Ballini, and H. van den Bergh, "An optical phantom with tissue-like properties in the visible for use in PDT and fluorescence spectroscopy," Phys. Med. Biol. **42**(7), 1415–1426 (1997).
28. T. J. Farrell and M. S. Patterson, "Diffusion Modeling of Fluorescence in Tissue," in *Handbook of Biomedical Fluorescence*, M. Mycek and B. W. Pogue eds. (CRC, 2003), pp. 29–60.
29. S. Yamaguchi and Y. Sasaki, "Spectroscopic determination of very low quantum yield of singlet oxygen formation photosensitized by industrial dyes," J. Photochem. Photobiol. Chem. **142**(1), 47–50 (2001).
30. M. A. Itzler, M. Entwistle, M. Owens, K. Patel, X. Jiang, K. Slomkowski, S. Rangwala, P. F. Zalud, T. Senko, J. Tower, and J. Ferraro, "Geiger-mode avalanche photodiode focal plane arrays for three-dimensional imaging LADAR," Proc. SPIE **7808**, 78080C (2010).
31. V. V. Russkikh, A. V. Konstantinova, V. N. Berezhnaya, T. N. Gerasimova, and V. V. Shelkovnikov, "Improved synthesis of thiofluorescein," Russ. J. Org. Chem. **41**(1), 57–60 (2005).
32. A. Chevalier, C. Mercier, L. Saurel, S. Orenga, P.-Y. Renard, and A. Romieu, "The first latent green fluorophores for the detection of azoreductase activity in bacterial cultures," Chem. Commun. (Camb.) **49**(78), 8815–8817 (2013).

1. Introduction

Singlet-oxygen ($^1O_2$) is a highly reactive state of molecular oxygen and plays an important role in many biological processes. Photodynamic therapy (PDT) relies on the generation of $^1O_2$ through the photoactivation of a photosensitive drug to selectively treat several types of pathologies like solid tumors, skin diseases, vascular disorders, and bacterial infections [1–5].

Dosimetry of $^1O_2$ during the treatment has been proposed to ensure that the optimal PDT dose is delivered to the patient. Consequently, considerable research and efforts have been undertaken to develop direct and indirect techniques enabling the measurement of the concentration of singlet-oxygen [6,7]. Direct dosimetry of $^1O_2$ can be achieved by measuring the luminescence in the near-infrared (NIR) range (1270 nm) of singlet-oxygen decay. However, due to the high reactivity of $^1O_2$ and the consequent low efficiency of the process (i.e. return to the ground state of $^1O_2$), resulting in light fluxes close to single-photon levels, direct dosimetry remains challenging.

Suitable single-photon detectors in this wavelength range have traditionally been limited to NIR photomultiplier tubes (PMTs) and deep-cooled InGaAs cameras. InGaAs cameras have good photon detection efficiency (> 30 – 50%) and large active areas (> 10 mm x

#251795 Received 14 Oct 2015; revised 17 Dec 2015; accepted 17 Dec 2015; published 23 Dec 2015

10 mm) but have no time-resolving capabilities. PMTs on the other side are the detector of choice in many singlet-oxygen experiments [8]. Their main advantage is a large active area (> 10 mm) that is essential to collect photons from large diffusing samples. Unfortunately, they have many disadvantages like very low quantum efficiency (< 1%), moderate noise (> 10000 cps), delicate photocathode (it can be damaged by ambient light) and the difficulty to gate the detector to suppress stray light during measurement.

In different regions of the visible and low NIR spectrum (400 nm – 1000 nm), silicon single-photon avalanche diodes (SPADSs) are replacing PMT thanks to their higher detection efficiency, lower noise, compact form factor, stability, ease-of-use and possibility to be gated. The active area is considerably smaller (20 μm – 500 μm) but it is often compensated by the other advantages especially if the sample has limited emission geometry (like in confocal microscopy [9], scanning systems [10] or fiber-based endoscopy [11]).

In the NIR wavelength range (1000 nm – 1700 nm) SPADs are also an emerging technology but their use is limited by high noise (Dark Count Rate, DCR) and to gated-mode operation with maximum gate widths of few tens of nanoseconds [12]. Some research has been done on the characterization of collagen in the NIR range [13] but SPADs have never been used for singlet-oxygen detection: in fact, they are not compatible with the long time constant of singlet-oxygen decay (> 40 ns *in vivo*, > 3 μs for aqueous solutions) and the low photon flux expected.

In the last decade, alternative detectors such as superconducting nanowire single-photon detectors (SNSPDS) working at cryogenic temperatures have been proposed for the NIR range. In a recent study, the use of an SNSPD [14] to measure singlet-oxygen luminescence has been reported, but the clinical exploitation is limited by size, cost and complexity.

Here, we propose a practical setup based on our recently-developed negative-feedback avalanche diode (NFAD) detector [15] that solves most of the challenges to create a clinically compatible instrument while improving the performance with respect to the state of the art.

We have demonstrated that these detectors can achieve DCR as low as 1 cps at 10% efficiency (at 1550 nm) [16]. These low DCR values, typically only achieved with SNSPDs, can open the door to applications previously not possible with SPADs. Furthermore, the detector proposed in this work is coupled to a large area multimode fiber (62.5 μm NA 0.275) which enhances the collection efficiency in biological samples both *in vitro* and *in vivo*. The collection efficiency is a factor of 100 higher with respect to a previously published result based on a single-mode fiber-coupled detector [14] developed for a similar application.

The driving electronics has also been designed to allow the operation of the detector either in free-running mode (detector always ON and ready to detect photons) or gated-mode (the detector can be selectively switched OFF to suppress unwanted light signals). The latter operating mode is particularly useful when the dim singlet-oxygen signal is measured in samples where a lot of stray photons, originating from fluorescence, are present.

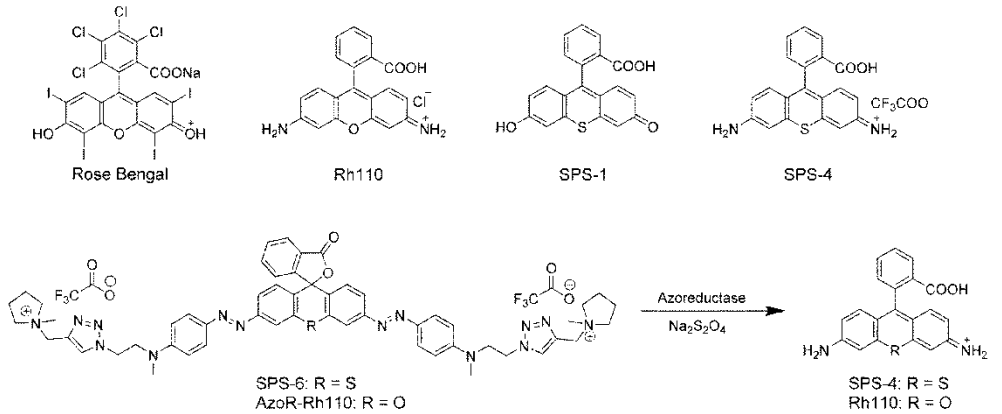

Fig. 1. Chemical structures of compounds and the activation of SPS-6 and AzoR-Rh110.

#251795 Received 14 Oct 2015; revised 17 Dec 2015; accepted 17 Dec 2015; published 23 Dec 2015

In this paper, we present results from the characterization of this novel setup for time-resolved singlet-oxygen luminescence detection (SOLD). Using Rose Bengal as a standard, we first assessed the performance of the setup in terms of collection efficiency, noise and gated-mode operation. Then, the setup was used to measure the singlet-oxygen quantum yield of a new series of photosensitizer prodrugs that have been developed for site-selective activation through azoreductase for localized antimicrobial PDT.

2. Materials and methods

2.1 Chemicals

Figure 1 shows the chemical structures of the compounds used in this paper. Rose Bengal is a commercially-available photosensitizer that we used in the initial characterization of the setup and as a reference photosensitizer due to the large literature available [17,18]. Rh110 is a rhodamine fluorescent dye from which we derived a series of new photosensitizers to be used for the site-selective treatment of bacterial infections. These compounds are photochemically inactive through photoinduced electron transfer [19]. However, in presence of a target enzyme these new compounds restore their fluorescence and singlet oxygen quantum yield. For the purpose of antibacterial treatment we have chosen azoreductases activity. This kind of enzymes catalyzes the reduction of azo compounds into amines [20]. They play an important role in the defense mechanism of bacteria against quinones [21]. Therefore, we have prepared aryl diazo derivatives of Rh110 that drives the xanthene platform into a non-fluorescent closed lactone form. In order to further increase the singlet-oxygen quantum yield through the heavy atom effect we have replaced the oxygen within the xanthene skeleton by sulfur. Compared to their selenium counterparts, these sulfur derivatives are still fluorescent in their activated form allowing control of their activation state through fluorescence measurements.

2.2. Determination of optical properties

2.2.1 Low-noise InGaAs/InP single-photon detector

Our setup is based on a commercially-available NFAD detector by Princeton Lightwave (model nr. E2G2) [22]. It features an integrated quenching resistor of approximately 500 kΩ that allows a very fast quenching of the avalanche current generated when a photon is detected and reduces the amount of charge flowing in the detector. This charge is proportional to one of the main sources of noise in InGaAs/InP detectors: after-pulsing noise [23]. Due to an active hold-off circuit, the after-pulsing probability is further reduced compared to traditional single-photon avalanche diodes and allows for free-running (always ON) operation of the detector and relatively high counting rates (> 50000 count-per-second, cps).

The detector is housed in a dry chamber and cooled with a free-piston stirling cooler (FPSC) (Twinbird SC-UE15R). The device used in this work was cooled to 183 K and features 72 cps of DCR with a dead-time of 20 μs. The photon detection efficiency (including the coupling to the multimode fiber pigtail) is 25.7% at 1310 nm (close to the singlet-oxygen emission spectrum (1270 nm)).

For this application, the driving electronics of the device have been designed to allow operation in a gated-mode. The detector is kept OFF during the pulsed laser excitation in order to reject stray photons from the laser or from short-lived fluorescence. With an external trigger signal (e.g. the laser electrical trigger signal), the detector can be turned ON with a user-selectable delay with respect to the excitation. This gated-mode operation, however, is very different from other gated SPADs since our detector can remain active for a sufficient time to collect the slow luminescence decay (i.e. for singlet-oxygen the life-time is >3 μs).

#251795 Received 14 Oct 2015; revised 17 Dec 2015; accepted 17 Dec 2015; published 23 Dec 2015

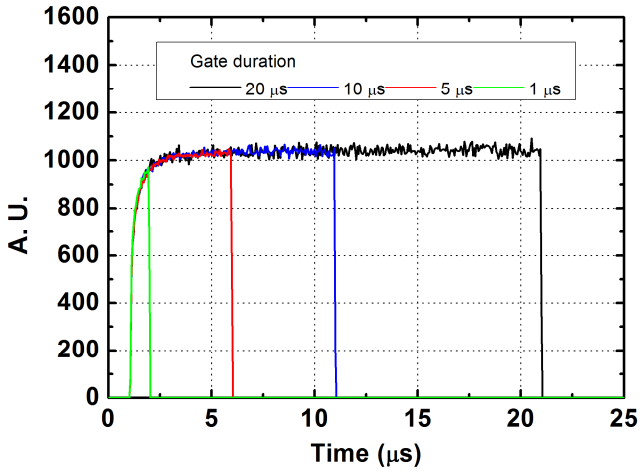

Fig. 2. Measurement of the shape of the gate signal of the detector obtained illuminating the active area with a constant light source at 532 nm. The rise time is approximately 1 μs (10-90%) and is limited by the intrinsic time constant of the internal quenching resistor of the avalanche diode and its parasitic capacitance.

The rise time of the gate signal (see Fig. 2) is limited by the integrated resistor and the parasitic capacitance of the diode and is approximately 1 μs (10 – 90%). We measured various gate durations from 1 μs to 20 μs with a repetition frequency of 40 kHz. The response of the detector is flat and the duration can be selected to accommodate even decay signals with long life-times.

2.2.2 Experimental setup

The experimental setup for time-resolved singlet-oxygen luminescence measurement is shown in Fig. 3 (left). Samples are contained in a 300 μL plastic cuvette. A Q-switched laser at 532 nm (Crystal Laser Inc. QG-532-1W) provides the excitation pulses (10 ns duration, 40 kHz repetition frequency, 200 mW average power). A first band-pass filter (BPF1, 532 nm center wavelength, 10 nm bandwidth, Thorlabs Inc., FL532-10, Newton, NJ, US) rejects any spurious out-of-band emission from the laser and a variable circular attenuator controls the average output power. A series of two lenses (Lens 1: f = 50.0 mm, D = 25.4 mm, Lens 2: f = 75.0 mm, D = 25.4 mm) acts as a beam expander and produces a collimated beam of 3 mm in diameter directed towards one of the two transparent sides of the cuvette. A dichroic mirror (Thorlabs Inc., DMLP-900, Newton, NJ, US) reflects the pump laser but transmits in the 1270 nm range. Emitted NIR photons are first collimated by the same Lens 2 and then focused on the detector fiber by a final lens (Lens 3: f = 25.4, D = 25.4 mm). The collection scheme has been optimized to have the collection efficiency limited only by the numerical aperture and diameter of the multimode fiber of the detector (NA = 0.275, D = 62.5 μm). In this way, it is possible to collect photons from an area of approximately 0.025 mm^2 with an equivalent numerical aperture of 0.1. A band-pass filter tuned at 1270 nm (BPF2, Thorlabs Inc., FB-1300-12, Newton, NJ, US) and a long-pass filter with a cut-off wavelength of 1200 nm (LPF1, Thorlabs Inc., FEL-1200, Newton, NJ, US) reject all unwanted photons. The laser provides the external trigger used as a START signal for a Time-to-Digital (TDC) converter (QuTools GmbH, QuTau, Munich, Germany). Then, the STOP signal is provided by the output of the NFAD detector that generates a digital pulse for every detected photon. Time-correlated single-photon counting (TCSPC) is used to measure the temporal shape of the detected luminescence signal [24]. The collected histogram is made of 10000 bins with a bin width of 2.4 ns.

#251795 Received 14 Oct 2015; revised 17 Dec 2015; accepted 17 Dec 2015; published 23 Dec 2015

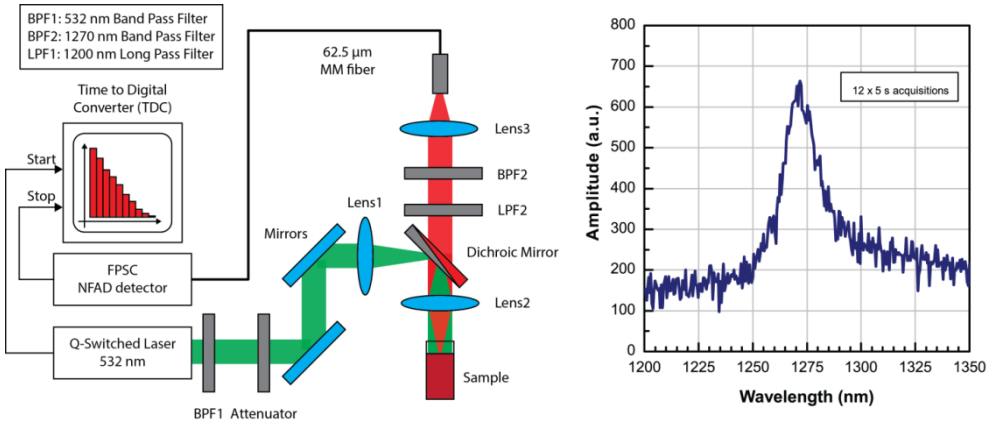

Fig. 3. (Left) Experimental setup used to detect the singlet-oxygen luminescence signal produced in different aqueous solutions of photosensitizer. The sample is excited with a 532 nm pulsed laser and the luminescence signal is collected through a confocal scheme. (Right) Spectrum obtained after LPF1 when measuring a standard photosensitizer drug (Rose Bengal). 12 consecutive acquisitions of 5 second each. The peak at 1272 nm is the typical signature of singlet-oxygen luminescence.

As a preliminary test, an aqueous solution of 10 µM Rose Bengal was prepared, BPF2 was removed and the excitation average power was set to 200 mW. A high-sensitivity electrically-cooled InGaAs CCD camera (Photonics Science Ltd., PSL High Sensitivity SWIR camera) was used with a self-made spectrometer to measure the emission spectrum of the sample. Figure 3 (right) represents the NIR spectrum resulting from the average of 12 acquisitions of 5 seconds each. A peak at approximately 1270 nm is distinguishable and is a clear indication of the emission of photons from singlet-oxygen decay.

3. Results

3.1 Time-resolved measurement with Rose Bengal dye

The performance of the developed NFAD detector was assessed with an aqueous solution (10 µM) of Rose Bengal used as a standard [17, 18]. The average output power of the excitation laser was set to 5 mW. Figure 4 shows the typical decay curve (blue line) of singlet-oxygen emission and is in agreement with previous works [8–14]. An intense and short-lived emission is measured during the first 1 µs. This has been attributed previously to the fluorescence of the optical elements of the setup and leakage of the excitation pulse into the detector [14].

Following background subtraction and removal of the initial signal, we estimate a signal of 1750 photons collected per second (350 cps/mW of pump laser). This is only a small portion of the emitted fluorescence (the numerical aperture of the system is 0.1) but it is sufficient to characterize the sample. The acquired detection rate is nonetheless comparable with a setup employing a large area NIR PMT [25]. This performance is highly dependent on the collection scheme, the laser repetition frequency, the optical power etc. However, a more direct comparison can be made with a recent, similar setup based on a superconducting nanowire single-photon detector (≈3 cps/mW of pump laser) [14]. In this case, our setup allows for an improvement of more than two orders of magnitude compared to the SNSPD-based one. The improvement is due to our higher collection efficiency and higher quantum efficiency of the detector.

It is also important to note that thanks to the higher efficiency, the power density on the sample (70 mW/cm^2) has been kept below the 100 mW/cm^2 typically used in a clinical trial and well below the threshold of 200 mW/cm^2 for *in vivo* treatment in humans [26].

To further prove the nature of the collected signal 50 µL of 2M Sodium Azide (NaN_3) were added to the sample in order to quench the singlet-oxygen production. Figure 4 (black

#251795 Received 14 Oct 2015; revised 17 Dec 2015; accepted 17 Dec 2015; published 23 Dec 2015

line) shows the measured signal. Only the spurious initial fluorescence is still present but the singlet-oxygen production has been completely quenched.

3.2 Gated measurement

In our sample model, the intensity of the spurious fluorescence signal was not a limiting factor with respect to saturation of the detector. However, in more complex systems (such as *in vivo*), many sources of unwanted photons can preclude the detection of the faint singlet-oxygen signal. Gating of the single-photon detector is a viable option to suppress spurious signals and has been already proven useful in other fields such as microscopy [9] or *in vivo* diffuse optical spectroscopy [10]. Figure 5 (left) shows the comparison of the singlet-oxygen decay measured with the detector in free-running mode (blue line) and in gated-mode (black line). In this case, the gate duration was set to 20 µs and delayed approximately 1 µs after the laser pulse. Except for the distortion of the signal in the first microsecond caused by the slow rise time of the detector, both curves are perfectly overlapping. To assess the distortion introduced by the gating system to the fluorescence curve, the same gate signal was applied at

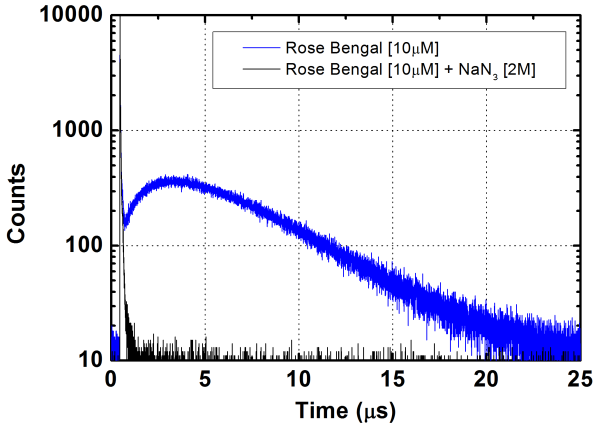

Fig. 4. Time-correlated single-photon counting acquisition of the singlet-oxygen luminescence decay of an aqueous solution of Rose Bengal dye before and after the addition of 2M Sodium Azide. 2.4 ns time-bin, 10000 bins. The pump power has been adjusted to 5 mW and the acquisition time is 600 s.

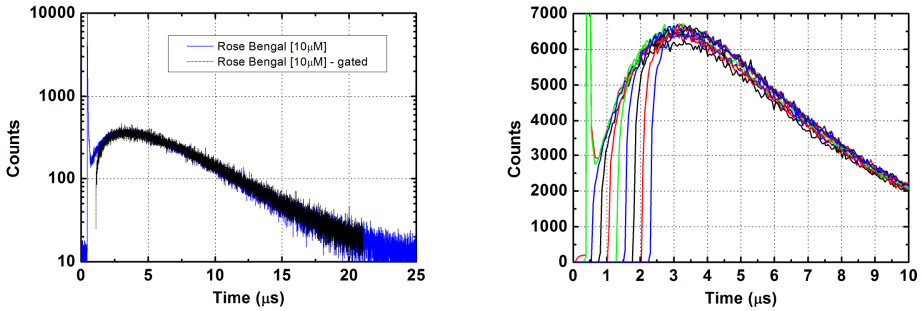

Fig. 5. (Left) Time-correlated single-photon counting acquisition of the singlet-oxygen luminescence decay of an aqueous solution of Rose Bengal dye with (black line) and without (blue line) gating applied to the detector (20 µs gate width). 2.4 ns time-bin, 10000 bins. The pump power has been adjusted to 5 mW and the acquisition time is 600 s. (Right) Zoom of the first 10 µs for 10 different delays (at 250 ns steps) between the gate signal and the laser pump. A 20-fold binning has been applied.

#251795 Received 14 Oct 2015; revised 17 Dec 2015; accepted 17 Dec 2015; published 23 Dec 2015

10 different delays from the laser pulse at steps of 250 ns and the result is recorded in Fig. 5 (right). For an easier identification of the curve, a 20-fold binning filter has been applied to the histograms. It is clearly visible that each curve is perfectly reconstructed and presents just a repeatable distortion due to gating rise-time. For long lifetimes this is not a problem: for lifetimes comparable with the rising edge of the gating signal, the shape of the gate can be acquired a priori and used to equalize the fluorescence curve since the detector response is stable with time. For this detector, the rising edge is mainly limited by the 500 kΩ resistor integrated in the NFAD structure and used to passively quench the current. There are no commercially-available detectors with a smaller integrated resistor but this is not at all a technological limitation. Rise times smaller than 50 ns could be achieved in the near future.

3.3 Detection of singlet-oxygen luminescence in a highly-diffusing optical phantom

To demonstrate the feasibility of singlet-oxygen detection with our detector in a scenario closer to a clinical case, we prepared an optical phantom as described in Appendix A [27]. It consists of a 3-layer structure where the bottom layer is a plain absorbing/scattering medium with 3 mm thickness, the middle layer is 1 mm thick and is dyed with 10 μM Rose Bengal photosensitizer and the top layer is a plain medium with a varying thickness of approximately 0 mm to 6 mm.

Two identically-prepared phantoms were illuminated for 60 s at an average power of 10 mW at three different positions for each thickness of the top layer, while a time-resolved fluorescence histogram was collected. Counts from each histogram were then integrated from 1.5 μs after the laser pulse (just before the peak of the fluorescence decay) up to 20 μs. A control phantom (without Rose Bengal) was also measured and used for background subtraction. Results are presented in Fig. 6: the collected luminescence signal decays with varying thickness of the optical phantom and it is still possible to collect an average of 10 cps with a 5 mm thickness above the photosensitizer layer. Moreover, we note that the singlet-oxygen luminescence signal does not decrease significantly up to a depth of 3mm. This behavior could be explained by a combination of the geometrical collection efficiency of the instrument together with the diffusion of light in the phantom and was observed and modeled in different scattering media [28].

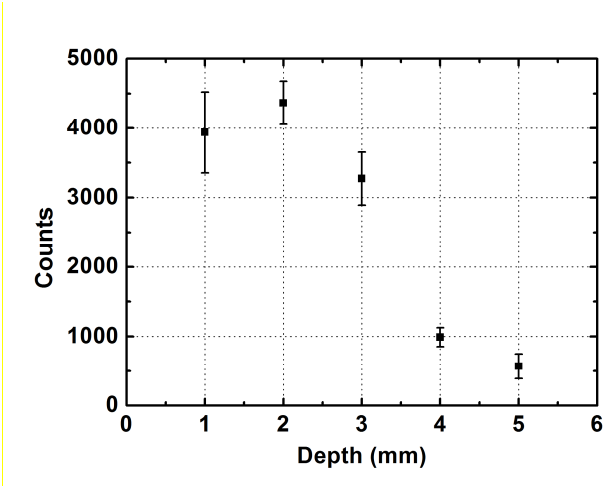

Fig. 6. Singlet-oxygen luminescence counts collected during 60 s of irradiation of an optical phantom with a central 1 mm thick layer dyed with 10 μm Rose Bengal and a superficial layer with varying thickness. The pump power was set to 10 mW. Singlet-oxygen luminescence can be detected up to a depth of 5 mm.

#251795 Received 14 Oct 2015; revised 17 Dec 2015; accepted 17 Dec 2015; published 23 Dec 2015

3.4 Characterization of site-selective photosensitizers

In this study, Rose Bengal was used as reference photosensitizer and its singlet-oxygen quantum yield is found in literature to be 76% in aqueous solution [17, 18]. By comparing the measured luminescence signal and normalizing for the absorption of a specific solution, it is possible to estimate the singlet-oxygen quantum yield through the NIR emission of a newly developed photosensitizer by comparing it with Rose Bengal, as according to Eq. (1):

$$\phi_{\Delta C} = \frac{A_{RB}}{A_C} \times \frac{ph_C}{ph_{RB}} \times \phi_{\Delta RB} \tag{1}$$

where $\phi_{\Delta C}$ and $\phi_{\Delta RB}$ are the singlet-oxygen quantum yield of the tested compound and Rose Bengal respectively, A_{RB} and A_C are the total absorptions of the samples at the wavelength of interest (532 nm in our case) and ph_C and ph_{RB} are the measured NIR photon rates.

We hence characterized our newly-developed compounds targeting site-selective photodynamic therapy and compared them with some reference molecules which should not exhibit fluorescence or singlet-oxygen production upon illumination.

Figure 7(a) and 7(c) show the absorption and fluorescence spectra of compounds AzoR-Rh110 and SPS-6 compared to their activated counterparts SPS-4 and Rh110. For all azo compouds, a hypsochromic (blue) shift of more than 70 nm of their principal absorption band can be observed. On the other hand, a bathochromic (red) shift is observed when comparing rhodamine and its corresponding thiol derivative. From Figs. 7(b) and 7(d) it can be seen that both diazo compounds are barely fluorescent in aqueous solution when exited at 518 nm.

Compound AzoR-Rh110 is 7000 times less fluorescent than its activated form. Also, SPS-6 is 10000 times less fluorescent then SPS-4. Activation was measured in the presence of

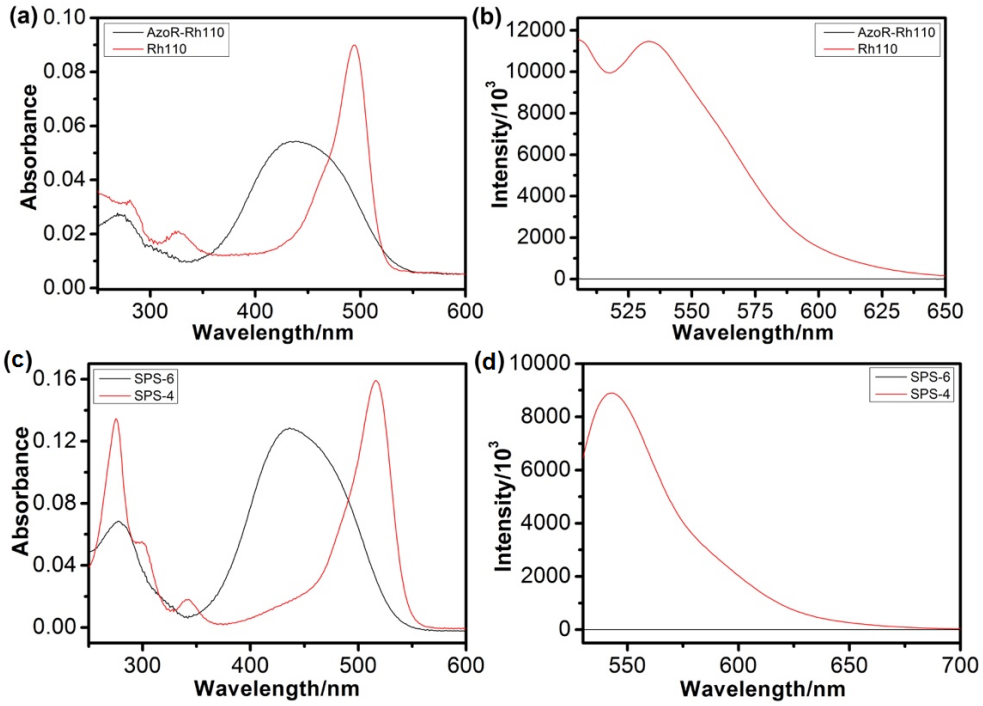

Fig. 7. Absorption (left) and fluorescence (right) spectra of compounds AzoR-Rh110 and SPS-6 (black lines) compared to their activated counterparts SPS-4 and Rh110 (red lines). An increase in the fluorescence of the activated compounds is clearly visible.

#251795 Received 14 Oct 2015; revised 17 Dec 2015; accepted 17 Dec 2015; published 23 Dec 2015

$Na_2S_2O_4$ as reducing agents. Within one minute a fluorescence increase of over 260 and 320 times was observed for AzoR-Rh110 (F_{520nm}) and SPS-6 ($F_{542\ nm}$), respectively. Figure 8, on the other hand, shows the measured singlet-oxygen luminescence decay curves for the various solutions (at a constant concentration of 10 µM). Although Rose Bengal has the highest luminescence signal, SPS-1 and SPS-4 show a clearly distinguishable signal as well.

In order to calculate the singlet-oxygen quantum yield we measured the absorption spectrum of the solutions under test to normalize the luminescence signal for the number of photons effectively absorbed. Figure 9 (left) shows the measured absorption spectra. Figure 9 (right) shows the calculated singlet-oxygen quantum yield. Rh110 has a singlet-oxygen quantum yield of 2% which is in agreement with quantum yields of other rhodamine derivatives. However, the sulfo derivatives, SPS-1 and SPS-4, show the expected singlet-oxygen quantum yield increase to 36% and 21% respectively. Most importantly, AzoR-Rh110 and SPS-6 show no measurable singlet oxygen fluorescence, proving that the molecule is effectively inhibited as a photosensitizer, when it is not activated.

To measure lower quantum yields (below 1 – 2%), the sensitivity of our current setup is limited by the photobleaching of the compounds for higher excitation powers and longer integration times. With stable dyes, increasing the pump power to 50 mW and for an integration time of 50 s, for example, a quantum yield of 0.1% could be measured with a SNR of 10. With other techniques, the estimation of quantum yields in the order of 0.1% – 0.01% was demonstrated using a modulated laser source and lock-in amplification (see e.g [29].). Unfortunately, these alternative techniques have only limited time-resolving capabilities and lack of selectivity in time.

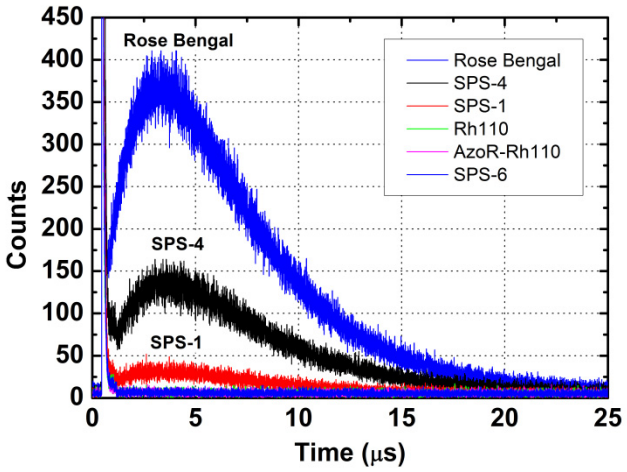

Fig. 8. Singlet-oxygen luminescence decay of different aqueous solutions [10 µM]: a commercially-available photosensitizer (Rose Bengal), a fluorescent dye (Rh110) and several novel photosensitizer molecules. 2.4 ns time-bin, 10000 bins. The pump power has been adjusted to 5 mW and the acquisition time is 600 s. The fluorescence signals from Rose Bengal, SPS-1 and SPS-4 are clearly visible; the other curves are close to the noise floor.

#251795 Received 14 Oct 2015; revised 17 Dec 2015; accepted 17 Dec 2015; published 23 Dec 2015

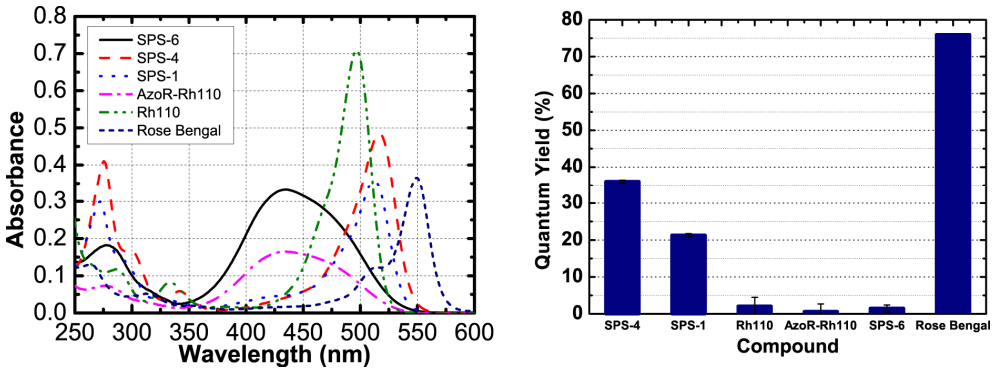

Fig. 9. (Left) Measured absorption spectra of the solutions, the wavelength used during the experiment is 532 nm. (Right) Calculated singlet-oxygen quantum yield of the different solutions. The quantum yield of Rose Bengal (76%) is used as a reference.

4. Conclusion

We presented for the first time a time-resolved singlet-oxygen luminescence detection setup based on a semiconductor single-photon detector. Exploiting a commercially-available diode, a free-piston Stirling cooler and dedicated driving electronics we were able to achieve a detection efficiency of around 25% at 1310 nm while maintaining low noise (approximately 70 cps at 183 K), high collection efficiency (thanks to the multi-mode fiber) and the possibility to work in gated-mode to selectively suppress spurious photons. Compared to setups based on NIR PMTs or superconducting detectors, we presented an instrument with the following characteristics: high quantum efficiency, low-noise, it is compact, low-cost, easily fiber-coupled to a large area fiber and it is easy to use.

We demonstrated a signal-to-noise ratio (SNR) improvement of over two orders of magnitude compared to superconducting detectors in a similar setup [14]. Compared to PMTs, instead, the smaller active area is easily compensated by the significantly higher quantum efficiency and lower noise in setups where geometrical collection efficiency cannot be exploited (like fiber-based setups, scanning systems, confocal microscopes etc.) The higher SNR allows for shorter acquisition time and lower excitation power that are fundamental for *in vivo* measurements.

We were able to measure the singlet-oxygen quantum yield of a series of new photosensitizers and compared them to commercially-available Rose Bengal. These compounds are being developed for site-selective photodynamic therapy of bacterial infections. They are activated by azoreductases and show a clear increase both in their fluorescence spectrum and singlet-oxygen quantum yield when they are activated.

Furthermore, the demonstration of the feasibility of using InGaAs/InP photodetectors for singlet-oxygen detection and dosimetry exposes this technique to a fast growing technology: it is, in fact, already possible to produce large area arrays of detectors [29] that could be used to perform direct imaging of the sample or be coupled to fiber bundles for in situ treatment and detection of solid tumors etc. We hence believe that this proof-of-principle work represents only the first step in the exploitation of emerging single-photon detection technologies in clinically-valuable applications such as photodynamic therapy.

Appendix A: optical phantom preparation

The optical phantom was adapted from a literature procedure [27]. Briefly, 3.0 g of Agar-Agar (Aldrich, Buchs, Switzerland), 40 mL of mQ water and 40 mL of DPBS were heated and boiled while stirring to dissolve the powder. Then, 3.0 g of 40-63 µm diameter silica powder (Silicycle, Québec, Canada) were added to the heated liquid and sonicated to homogenize the solution. A 1 mM stock solution of Rose Bengal (Fluka, Buchs, Switzerland) in mQ water was prepared aside. To 10 mL of the agar-agar solution were added 100 µL of

#251795 Received 14 Oct 2015; revised 17 Dec 2015; accepted 17 Dec 2015; published 23 Dec 2015

the solution of Rose Bengal to reach a final concentration of 10 μM. Each layer is then poured into a different Petri dish (55 mm diameter). The first layer (3 mm of thickness) is made of the solution without Rose Bengal, the second layer (1 mm of thickness) is made of the solution with Rose Bengal, and the third layer (from 0 to 6 mm of thickness) is made of the solution without Rose Bengal. Each layer is cooled at 4 °C during one hour before the assembly. Then, the three layers were assembled together in a Petri dish with a polyethylene film between each of the layers to prevent any passive diffusion of the Rose Bengal. A control was made on the same model, but the central layer was without Rose Bengal.

Appendix B: general experimental procedures

Abbreviations. The following abbreviations are used: AzoR, azoreductase; Rh110, rhodamine 110; DMF, N,N-dimethylformamide; DMSO, dimethylsulfoxide; EtOAc, ethyl acetate; DCM, dichloromethane; THF, tetrahydrofurane; Xantphos, 4,5-Bis(diphenylphosphino)-9,9-dimethylxanthene; PhN(Tf)2, N-Phenyl-bis(trifluoromethanesulfonimide); Pd_2dba_3, Tris(dibenzylideneacetone)dipalladium(0); NOBF4, Nitrosyl tetrafluoroborate; NaAsc, sodium ascorbate; DIEA, N,N-Diisopropylethylamine; TEA, triethylamine; TFA, trifluoroacetic acid; DPBS, Dulbecco's Phosphate-Buffered Saline; r.t., room temperature; ESI, electrospray ionisation; RP-HPLC, reversed-phase high performance liquid chromatography.

Reagents and Apparatus. All chemicals were purchased from Alfa Aesar, Acros or Sigma-Aldrich and were used as received. DPBS was purchased from Invitrogen AG Lifetechnologies. All solvents were purified using standard procedures. ^{1}H NMR spectra were recorded on a Bruker AVANCE-400 spectrometer and referenced to solvent signals. Mass spectra (ESI) were obtained on ESI API 150 EX. The pH values were measured by a 691 pH Meter from Metrohm. UV-visible spectra were recorded on Cintra 404 UV-vis spectrometer from GBC Scientific Equipment Ltd. Fluorescence spectra were recorded using a FluoroMax-4 spectrometer from Horiba Scientific. The path length was 1 cm with cell volume of 2.0 mL using quartz cuvette. The scanning was carried out with an integration time of 0.2 s, an excitation/emission spectral slit of 2.5 nm and an accumulation of 3 scans. All of the spectroscopic measurements in this supporting information were carried out in phosphate-citrate buffer (20 mM NaH_2PO_4 and 20 mM citric acid, 25 °C) or DPBS buffer solution.

Stock solution of all the dyes was prepared in DMSO (2.0 mM) and stored at −20 °C. Aq. solution $Na_2S_2O_4$ was prepared fresh every time before use.

Appendix C: synthesis of compounds

Thiofluorescein (SPS-1), N-(2-Azidoethyl)-N-methylaniline (1), alkyne-functionalised pyrrolidinium salt (2) and AzoR-Rh110 were synthesized according to known procedures [30,31]. The synthesis of compounds SPS-2, SPS-3, SPS-4, SPS-5 and SPS-6 is represented in Fig. 10.

Compound SPS-2. A solution of SPS-1 (0.67 g, 1.92 mmol) and $PhN(Tf)_2$ (2.48 g, 6.94 mmol) in dry THF (30 mL) was stirred under argon at r.t. overnight after addition of DIEA (2.40 mL, 13.78 mmol) dropwise. Then the solvent was evaporated, and the crude product was further purified by flash chromatography (silica gel, hexane/0-50% DCM) to give pure compound SPS-2 (0.94 g). Colorless oil, Yield: 80%. ^{1}H NMR (300 MHz, DMSO-d_6, ppm): 8.17 – 8.00 (m, 2H, C(O)-C-**CH** and C(O)-C=C-CH=**CH**), 7.92 – 7.85 (m, 1H, C(O)-C=C-**CH**), 7.85 – 7.63 (m, 1H, C(O)-C-CH=**CH**), 7.51 – 7.32 (m, 4H, C(O)-**CH**=**CH**), 7.32 – 7.21 (m, 2H, C(O)-**CH**-C). ESI: 613.3 ($M + H^+$).

Compound SPS-3. A vial was charged with **SPS-2** (160 mg, 0.26 mmol), tert-butyl carbamate (45 mg, 0.81 mmol), Pd_2dba_3 (32 mg, 0.035 mmol), Xantphos (47 mg, 0.081mmol) and Cs_2CO_3 (348 mg, 1.07 mmol). The vial was then sealed and evacuated/backfilled with argon (3×). Dry dioxane (12 mL) was added to be red solution and the reaction was stirred at 100 °C overnight. It was then cooled to room temperature, filtered through celite with DCM and evaporated to be yellow oil. The crude product was further purified by flash chromatography (silica gel, Petro Ether/0-30% EtOAc) to give pure compound **SPS-3** (95

#251795 Received 14 Oct 2015; revised 17 Dec 2015; accepted 17 Dec 2015; published 23 Dec 2015

mg). Colorless solids, Yield: 67%. ^{1}H NMR (400 MHz, DMSO-d_6, ppm): 9.63 (s, 2H, **NH**), 7.97 (d, J = 7.6 Hz, 1H, C(NH)-**CH**-C), 7.84 – 7.75 (m, 3H, C(NH)-**CH**-C and C(O)-C=C-**CH**=**CH**), 7.71 (t, J = 7.3 Hz, 1H, C(O)-C-CH=**CH**), 7.62 (d, J = 7.7 Hz, 1H, C(O)-C-**CH**), 7.23 (dd, J = 8.8, 2.1 Hz, 2H, C(NH)-**CH**=CH), 6.90 (d, J = 8.8 Hz, 2H, C(NH)-CH=**CH**), 1.47 (s, 18H, **CH_3**). ESI: 547.3 ($M + H^+$).

Compound SPS-4. SPS-3 (59 mg, 0.11 mmol) was dissolved in DCM (5 mL) to be colorless solution. Upon addition of TFA (1 mL), it became orange-red solution and was stirred at r.t. for 2h. Then the solvent was co-evaporated with EtOAc to obtain red solids. Purification of the residue by RP-HPLC (eluent, a 30-min linear gradient, from 10% to 100% solvent B; flow rate, 9.0 ml/min; detection wavelength, 500 nm; eluent A (H_2O containing 0.1% TFA (v/v)) and eluent B (CH_3CN containing 0.1% TFA (v/v))) provided **SPS-4** as trifluoroacetic salt (41 mg). Red solids, Yield: 82%. ^{1}H NMR (400 MHz, $CDCl_3$, ppm): 8.33 (dd, J = 7.7, 1.2 Hz, 1H, COOH-C-CH=CH-**CH**), 7.80 (m, 2H, COOH-C-**CH** and COOH-C-CH=**CH**), 7.39- 7.31 (m, 1H, COOH-C=C-**CH**), 7.18 (d, J = 9.3 Hz, 2H, $C(NH_2)$-CH=**CH** and C(NH)-CH=**CH**), 7.12 (d, J = 2.2 Hz, 2H, $C(NH_2)$=**CH**-C and C(NH)-**CH**=C), 6.83 (dd, J = 9.3, 2.2 Hz, 2H, $C(NH_2)$-**CH**=CH and C(NH)-**CH**=CH) (4 H missing). ESI: 347.5 ($M + H^+$).

Compound SPS-5. SPS-4 (59 mg, 0.13 mmol) was dispersed in a mixture of dry CH_3CN/DMSO (1.5 mL / 2.0 mL, v/v) to be red solution. TEA (36 µL, 0.26 mmol) was added and the mixture was stirred under argon at 0 °C until complete dissolution of **SPS-4**. Then, solid $NOBF_4$ (51 mg, 0.44 mmol) was added in one portion and the resulting reaction mixture was stirred vigorously at 0 °C for 15 min. Thereafter, N-(2-Azidoethyl)-N-methylaniline (**1**) (60mg, 0.34 mmol) in dry CH_3CN (2.0 mL) was added slowly to the pre-formed N-nitrosamine/diazonium salt intermediate and the resulting reaction mixture was stirred from 0 °C to r.t. under argon overnight. The solvent was evaporated and the crude product was further purified by flash chromatography (silica gel, petrol ether/0-40% EtOAc) to give pure compound (58 mg). Red oil, Yield: 74%. ^{1}H NMR (300 MHz, DMSO-d_6, ppm): δ 8.07 – 7.97 (m, 2H, **CH**=**CH**-**CH**=**CH**), 7.80 (dd, *J* = 9.7, 2.7 Hz, 4H, N(CH_3)-C-CH=**CH**), 7.69 (ddd, *J* = 20.4, 8.2, 1.9 Hz, 4H, N=N-C-**CH** and N=N-C=**CH**), 7.34 (d, *J* = 8.5 Hz, 2H, S-C=C-**CH**), 6.96 – 6.85 (m, 4H, N(CH_3)-C=**CH**), 3.72 (dt, *J* = 23.4, 5.8 Hz, 4H, N_3-CH_2-**CH_2**), 3.56 (dt, *J* = 15.3, 5.9 Hz, 4H, N_3-**CH_2**), 3.14 (s, 2H, N-**CH_3**), 3.06 (s, 4H, N-**CH_3**) (2H missing). ESI: 721.3 ($M + H^+$).

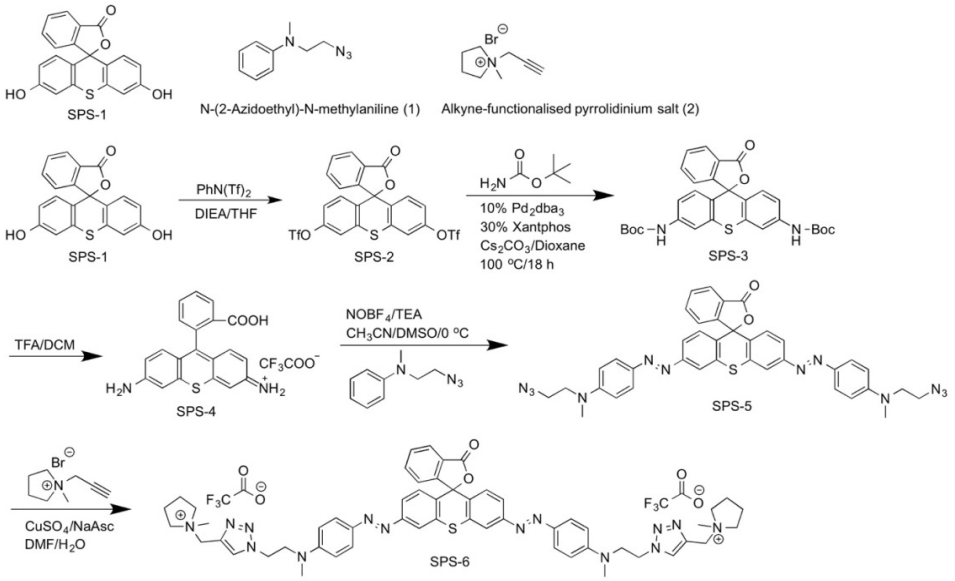

Fig. 10. Synthesis of compounds.

#251795 Received 14 Oct 2015; revised 17 Dec 2015; accepted 17 Dec 2015; published 23 Dec 2015

Compound SPS-6. SPS-5 (34 mg, 0.047 mmol) was dissolved in DMF (6 mL) together with Alkyne-functionalised pyrrolidinium salt (**2**) (59 mg, 0.29 mmol) in water. Aq. solutions $CuSO_4$ and NaAsc were added and the resulting reaction mixture was stirred under argon at 50 °C for 1 h and r.t. overnight. Then the solvent was evaporated to obtain red solids. Purification of the residue by RP-HPLC (eluent, a 40-min linear gradient, from 5% to 100% solvent B; flow rate, 9.0 ml/min; detection wavelength, 500 nm; eluent A (H_2O containing 0.1% TFA (v/v)) and eluent B (CH_3CN containing 0.1% TFA (v/v))) provided **SPS-6** as trifluoroacetic salt (20 mg). Red solids, Yield: 40%. ^{1}H NMR (400 MHz, DMSO-d_6, ppm): 8.39 (s, 2H, N-**CH**), 8.06 (d, *J* = 7.6 Hz, 1H, C(O)-C-**CH**), 8.03 (d, *J* = 2.0 Hz, 2H, S-C-**CH**), 7.88-7.81 (m, 2H, CH=**CH**-**CH**=CH), 7.79-7.75 (m, 1H, C(O)-C=C-**CH**), 7.73 (d, *J* = 9.1 Hz, 4H, N(CH_3)-C=CH-**CH**), 7.69 (d, *J* = 1.9 Hz, 1H, N=N-C-**CH**=CH), 7.67 (d, *J* = 2.0 Hz, 1H, N=N-C-**CH**=CH), 7.37 (d, *J* = 8.6 Hz, 2H, S-C=C-**CH**), 6.73 (d, *J* = 9.3 Hz, 4H, N(CH_3)-C=**CH**), 4.73 (t, *J* = 5.5 Hz, 4H, N-**CH_2**), 4.59 (s, 4H, N^+-**CH_2**-C), 4.02 (t, *J* = 5.2 Hz, 4H, N(CH_3)-**CH_2**), 3.22-3.12 (m, 8H, N^+-**CH_2**-CH_2), 2.98 (s, 6H, N^+-**CH_3**), 2.78 (s, 6H, N-**CH_3**), 2.08-1.90 (m, 8H, N^+-CH_2-**CH_2**). ESI: 484.5 (M^{2+}).

Acknowledgments

We would like to thank Luigi Bonacina for the Q-switched laser and for useful discussions. H. Zbinden acknowledges the Swiss NCCR QSIT for financial support. N. Lange's research is supported by the research grants 31003A_149962, 310000-109402, CR32I3_129987, 205320_138309; 205321_126834, and CR32I3_147018 from the Swiss Science Foundation.

#251795 Received 14 Oct 2015; revised 17 Dec 2015; accepted 17 Dec 2015; published 23 Dec 2015